

Effect of the Molecular Conformation on Excitation Energy Transfer in Conformationally Constrained Boryl-BODIPY Dyads

Rajendra Prasad Nandi, Chinna Ayya Swamy P,* Pandi Dhanalakshmi, Santosh Kumar Behera, and Pakkirisamy Thilagar*

Cite This: *Inorg. Chem.* 2021, 60, 5452–5462

Read Online

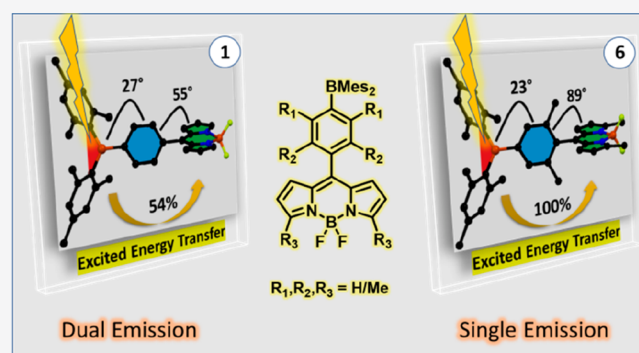
ACCESS |

Metrics & More

Article Recommendations

Supporting Information

ABSTRACT: We studied the dual emission characteristics of a series of boryl-BODIPYs (1–6) comprised of triarylborane (TAB) as an energy donor and BODIPY as an energy acceptor. The molecular conformations of dyads 1–6 were systematically tuned by judiciously changing the spacer that bridged the boryl and BODIPY moieties. Frontier molecular orbitals (FMOs) are localized in 3, 4, and 6 with a twisted molecular conformation. In contrast, FMOs are significantly delocalized in 1, 2, and 5 with the least-twisted molecular conformation. Dyads 1–6 showed dual emission features when they were excited at the TAB-dominated absorption band. However, the ratio between the two emission bands in 1–6 significantly varied depending on the molecular conformations. Systematic photoluminescence (PL) studies (both steady-state and time-resolved PL) together with computational, crystal structure, and anion binding studies established that the frustrated excited-state energy transfer from borane to BODIPY is the cause of the dual emission features in these molecular dyads. These studies also revealed that the energy transfer from borane to BODIPY can be elegantly tuned by modulating the dihedral angle between these two moieties.



INTRODUCTION

In recent decades, dual-emissive organic and organometallic compounds have received a lot of research interest, owing to their potential applications in displays, optical devices, sensing, and bioimaging.^{1–7} Therefore, an understanding of the underlying fundamental aspects that cause dual emission in organic and organometallic molecules is crucial to advance their functional application. Dual emissions such as dual phosphorescence,^{8,9} fluorescence phosphorescence,^{8,10–13} TADF phosphorescence,^{14–16} and dual TADF emission¹⁷ involving both singlet and triplet states have increasingly been reported in recent literatures. Continuous research efforts have uncovered that photoinduced electronic processes, such as intramolecular charge transfer (ICT),^{18,19} twisted ICT (TICT),^{20–22} excited-state intramolecular proton transfer (ESIPT),^{23–25} excited energy transfer (EET),^{26–28} trigger dual emission in organic and organometallic compounds.²⁹

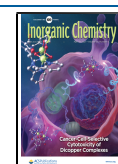
Among all these, the excited-state energy transfer (EET) process has been extensively exploited to develop broad emissive molecules and materials.^{30–32} The rate of energy transfer from an excited donor (D) to an energy acceptor (A) is governed by parameters such as the spectral overlap between the absorption and emission of A and D, the distance between D and A, the interchromophore orientation factor (k), etc.^{27,33–35} In the last two decades, numerous D–A systems

have been developed to understand the underlying mechanism in the EET process.^{36–43} In recent decades, the study of how external stimuli affect EET in covalently linked D–A systems has received a lot of attention due to their potential sensing applications. However, knowledge of external stimuli that affect EET in covalently coupled D–A systems is limited partly because of the difficulties in designing a versatile D–A system that can exhibit different optical signatures in the presence and absence of a stimulus.

Recently, a new type of D–A system comprised of tri- and tetracoordinate boron, such as triarylborane (TAB) and difluoroborondipyrromethene (BODIPY), has received considerable attention. The boron center in TAB is coordinatively unsaturated, inherently electron-deficient, and a Lewis acid. TAB can expand its coordination from three to four and effectively modify its structure and optical properties in the presence of suitable nucleophiles.^{7,44,45} On the other hand, BODIPY is a strongly luminescent dye that behaves as an

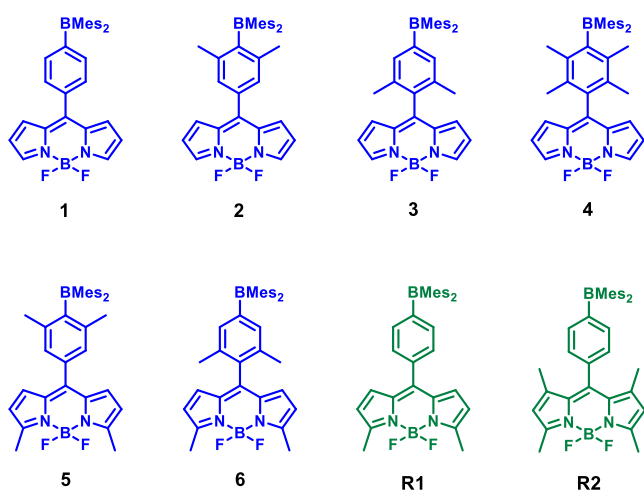
Received: September 14, 2020

Published: April 8, 2021



electron-donor or an electron-acceptor depending on the substituents attached.^{46–49} Covalently linked TAB and BODIPY conjugates would be ideal systems to understand the effect of external stimuli on the EET process because of the presence of a receptor (coordinatively unsaturated TAB) and strongly luminescent reporter BODIPY moieties. As proof of concept, we and others independently demonstrated the effect of nucleophiles, such as fluoride or cyanide, binding on the EET in different TAB-BODIPY dyads.^{7,50–57} During these studies, we have developed dual-, tricolor-, and white-light-emissive TAB-BODIPY conjugates.^{7,55,58,59} As a part of the ongoing program, we aim to investigate how finely one can tune the EET process in TAB-BODIPY dyads.⁶⁰ In this work, we have designed and synthesized a series of dyads (Chart 1)

Chart 1. Chemical Structures of the Newly Synthesized Boryl-BODIPY dyads 1–6 and Reference Compounds R1 and R2⁵⁹

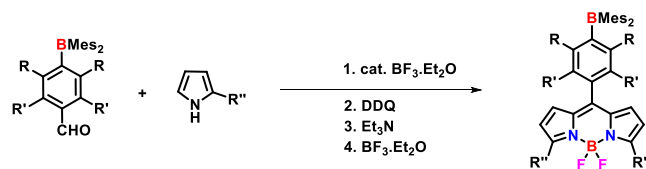


where the distance between the energy donor borane and the energy acceptor BODIPY was kept constant ($-C_6H_4-$). However, the molecular conformations were perturbed systematically by changing the dihedral angle between the D and A moieties by introducing steric crowding at the donor, acceptor, or spacer moieties. This study revealed that dyads with less sterically demanding spacers show dual emissions with a different PL intensity, whereas dyads with large sterically demanding spacers show predominantly a single emission. These intriguing results are summarized in this manuscript.

RESULTS AND DISCUSSION

Synthesis and Characterization. Boryl-benzaldehydes **a1–a4** were synthesized following the procedure reported elsewhere^{59,61} (see the [Supporting Information](#) for the detailed synthesis procedures). Boryl-BODIPY dyads **1–6** were prepared analogously from the respective boryl-benzaldehydes following the method recently reported by us.⁶⁰ In short, Lewis acid-mediated condensation of boryl-benzaldehydes (**a1–a4**) with pyrrole (pyrrole for **1–4** and 2-methyl pyrrole for **5** and **6**), followed by oxidation with DDQ and subsequent complexation with $BF_3 \cdot Et_2O$ in the presence of Et_3N , gave the desired compound (Scheme 1). Analytically pure **1–6** were obtained by passing the crude products through a neutral alumina column using hexane and ethyl acetate mixtures (9.8:0.2 ratio) as the eluent. Compounds **1–6** were purified as red-colored solids and characterized by NMR (1H , ^{13}C , ^{11}B ,

Scheme 1. Synthesis and Chemical Structures of 1–6



Compound	R	R'	R''
1	H	H	H
2	Me	H	H
3	H	Me	H
4	Me	Me	H
5	Me	H	Me
6	H	Me	Me

and ^{19}F) and HRMS techniques (Figure S1–S46). The molecular structures of all the compounds except **5** were characterized by single-crystal X-ray diffraction studies.

As expected, all the compounds showed two distinct ^{11}B NMR signals corresponding to tri- and tetra-coordinate boron in the regions at ~ 65 – 70 and ~ 0 – 2 ppm, respectively. The ^{11}B resonances in **3**, **4**, and **6** were shifted upfield compared to those in **1**, **2**, and **5**. In the ^{19}F NMR spectra, **1–6** showed a typical quartet for the boron-bound fluorines in BODIPY at ca. -146 ppm. The ^{13}C signal corresponding to the carbons attached to the boron could not be observed due to the fast relaxation of the quadrupolar boron nuclei. The number of ^{13}C and 1H NMR signals and the corresponding integration values were consistent with these compounds' molecular structures. ^{11}B and ^{19}F resonances of these compounds are comparable with those of TAB-BODIPY dyads reported elsewhere.^{50,51,56,59}

Theoretical Modeling Studies. Density functional theory (DFT) computational studies were performed on **1–6** to investigate the effect of their molecular conformations on the electronic communication between the boryl and BODIPY chromophores. DFT calculations were carried using a B3LYP hybrid functional and a 6-31G(d) basis set for all the atoms as incorporated in the Gaussian 09 software.⁶² All the molecules were optimized to their minimum potential-energy surface in the ground state, and corresponding frequency calculations were also carried out.

Figure 1 shows the frontier molecular orbitals (FMOs) of dyads **1–6** in their ground-state optimized geometries. The dihedral angle between the *meso*-phenyl ring (spacer) and the BODIPY core is an essential factor that determines the nature of the electronic communication between the boryl and BODIPY. The relative dihedral angles between the aryl spacer and the BODIPY ring were correlated to the extent of rigidity and conjugation around the BODIPY fluorophore. The calculated dihedral angles for **3**, **4**, and **6** were close to 90° due to two methyl groups on the spacer that were closer to the *meso*-carbon of BODIPY. In contrast, smaller angles were observed in **1**, **2**, and **5** with less sterically demanding spacers. In compounds **3**, **4**, and **6** that have larger dihedral angles, the highest occupied molecular orbitals (HOMOs) and the lowest unoccupied molecular orbitals (LUMOs) are mainly localized over BODIPY, indicating that the lowest electronic transition is centered on the BODIPY core. Meanwhile, the HOMO -1 and LUMO $+1$ orbitals are mainly localized over the borane moiety, suggesting the second possible transition centered on the TAB moiety. However, in compounds **1**, **2**, and **5** without methyl substituents in the spacer closer to the *meso*-carbon of

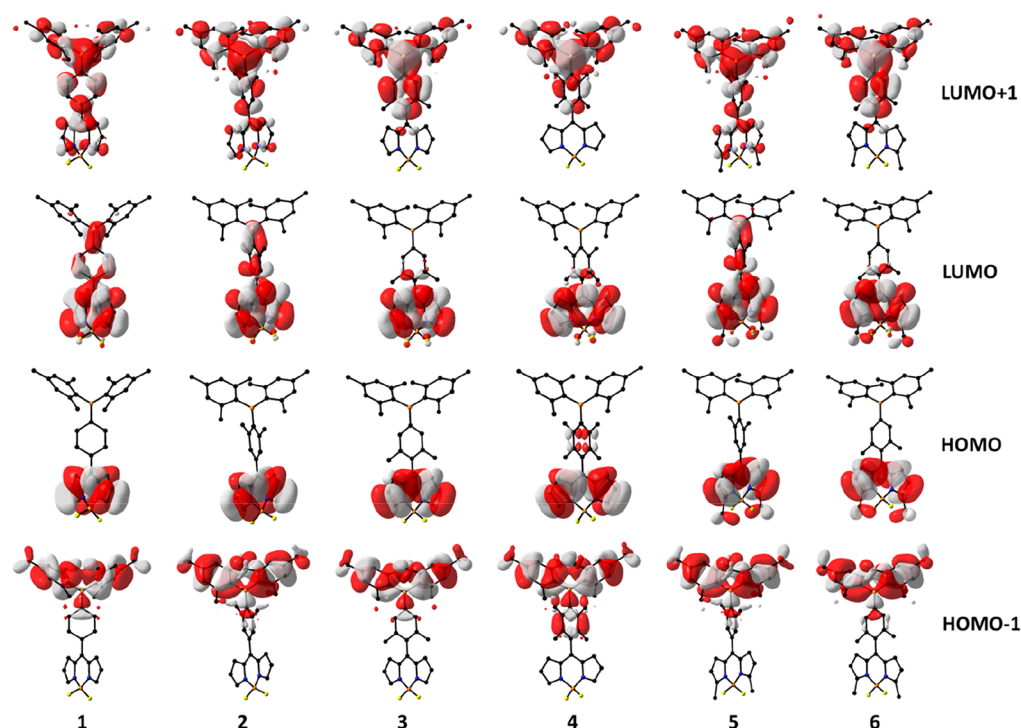


Figure 1. FMOs of 1–6 (left to right) obtained from the DFT level of theory using the B3LYP hybrid functional and the 6-31G(d) basis set for all the atoms as incorporated in the Gaussian 09 software (iso value of 0.02).⁶² Atom color codes are as follows: C, black; B, orange; and N, blue. Hydrogen atoms are omitted for clarity.

BODIPY, the LUMO and LUMO + 1 orbitals are delocalized compared to their HOMO (localized on BODIPY) and HOMO – 1 (localized on borane) orbitals. Orbital coefficient distributions in FMOs of 1, 2, and 5 are comparable with R1 devoid of substituents on the phenyl spacer, whereas 3, 4, and 6 behave like R2 with larger twist angles between the TAB and BODIPY moieties. Compounds 1, 2, and 5 with diffused FMOs are expected to show red-shifted absorption bands compared to those of 3, 4, and 6 with localized FMOs.

These results collectively imply that the molecular conformation significantly affects the FMOs of these dyads. Further, the noncrossing FMOs in 3, 4, and 6 are expected to show better energy transfer from TAB to BODIPY than 1, 2, and 5 with diffused FMOs. Thus, much like R1 and R2, the UV–vis absorbance spectra of 1–6 are expected to be like the additive spectrum of their respective isolated TAB and BODIPY moieties. However, emission properties may vary depending upon the modification in the excited states.

To further understand the nature of the electronic structure and molecular conformations of dyads, an analysis of the bond lengths was highly informative (Table 1). The C(spacer)–C(BODIPY) bond length is useful to qualitatively understand the conformational flexibility of the BODIPY core compared to that of the aryl spacer. As depicted in Table 1 for the DFT-optimized structures of 1, 3, 6, R1, and R2, C(Boryl)–C(spacer) distances (~ 1.575 Å) are shorter than those of 2, 4, and 5 (~ 1.595 Å). At the same time, C(spacer)–C(BODIPY) distances in 1, 2, 5, and R1 (~ 1.482 Å) are much more compressed than those in 3, 4, 6 (two methyl groups on the spacer toward BODIPY), and R2 (~ 1.497 Å). Compound 4 shows a significant elongation in both the C(spacer)–C(Boryl) (1.598 Å) and C(spacer)–C(BODIPY) (1.499 Å) bonds due to the sterically hindered duryl spacer. Thus, the

presence of additional methyl groups twisted the molecules and consequently localized the FMOs in these systems.

DFT calculations were also carried out for all the molecules in the solvated state (in dichloromethane) using a B3LYP hybrid functional and a 6-31G(d) basis for all the atoms as incorporated in Gaussian 09 software.⁶² Corresponding frequency calculations confirmed the optimization in their minimum potential-energy surface in the ground state. The comparison of metric parameters and FMO energy levels between the gas- and solution-phase calculations indicates minimum changes, as shown in the Supporting Information (Table S8–S12).

Single-Crystal X-ray Diffraction Studies. Single crystals of 1, 2, 3, 4, and 6 were obtained from the slow evaporation of their respective solutions in a pentane and chloroform mixture (5:1). Compounds 1, 2, and 4 were crystallized in the triclinic crystal system with the $P\bar{1}$ space group, whereas 3 and 6 were crystallized in the monoclinic crystal lattice with $P2_1/n$ and $P2_1/c$ space groups, respectively (Figures 2 and S53–S58, Tables S1 and S2). The structural parameters obtained from the single-crystal X-ray analysis are very similar to those of the DFT optimized structures (Table 1), and similar inferences can be drawn by analyzing these parameters. The slight deviation in the values of the bond parameters and dihedral angles may be due to solid-state packing and the associated intermolecular interactions in the crystal lattice. The tricoordinate boron center adopted trigonal planar geometry in all the compounds with a sum of the three C–B–C angles being 360° . For 3, 4, and 6, the dihedral angle between the spacer and BODIPY is $\sim 88^\circ$, whereas much smaller angles were observed in 1 (58.18°) and 2 (51.27°). This result clearly indicated that the methyl substituent on the spacer and the BODIPY moiety orthogonalized the BODIPY and TAB moieties. In summary, the combined crystallographic and

Table 1. Important Bond Length and Bond Angles^a

compounds	DFT-optimized structure (gas phase)				molecular structure from SCXRD			
	bond distance (Å)		dihedral angle (deg)		bond distance (Å)		dihedral angle (deg)	
	B(borane)–C(spacer)	C(BODIPY)–C(spacer)	BC2–spacer	BODIPY–spacer	B(borane)–C(spacer)	C(BODIPY)–C(spacer)	BC2–spacer	BODIPY–spacer
1	1.576	1.482	27.23	54.90	1.581	1.496	30.45	58.18
2	1.593	1.481	53.05	54.30	1.580	1.472	52.69	51.27
3	1.574	1.497	28.25	88.61	1.582	1.504	31.48	82.53
4	1.598	1.499	57.60	88.19	1.584	1.496	60.08	88.05
5	1.592	1.483	52.51	55.95	nd	Nd	nd	nd
6	1.576	1.497	23.08	89.53	1.558	1.494	25.74	81.72
R1	1.575	1.484	27.03	55.81	1.568	1.479	37.14	62.16
R2	1.577	1.495	21.39	88.80	1.567	1.468	31.22	77.74

^aR1 and R2 were reported in our previous report, BC2 indicates the plane comprised of B and two C atoms of two mesityl groups connected with B, and nd stands for not determined.

DFT analyses suggest that **1** and **2** are relatively more flexible than **3**, **4**, and **6**. The systematic steric perturbation is highly useful for fine-tuning the molecular conformation and the FMOs of the dyads.

Photophysical Properties. Compounds **1–6** exhibited similar absorption spectral features, with two major peaks at ~350 and ~520 nm and a shoulder peak at ~475 nm (Figures 3, S58, and S59). Model compounds (Chart 2) M4–M7 showed absorption peaks at ~310–330 nm, whereas M1–M3 showed absorption peaks at ~350 and ~500 nm with a shoulder at ~455 nm (Figures 4, S66, and S83).

Despite the direct attachment of TAB with the BODIPY moiety, the electronic interactions between these moieties were weak, and the absorption bands corresponding to individual molecular subunits can be recognized in their spectra of dyads. Thus, the absorption spectra of **1–6** are additive spectra of both TAB and BODIPY model compounds (M1–M3 and M4–M7, respectively (Chart 2)). These results indicated that linking TAB units at the *meso*-carbon of BODIPY does not affect the ground and Franck–Condon excited states of the individual chromophores. Similar absorption features have been reported for R1 and R2 with similar molecular constituents.

Even though the absorption bands may be ascribed to the distinct molecular components of the dyads, the electronic communications among them are not negligible. The absorption bands in **1**, **2**, **5**, R1, and R2, which are devoid of –CH₃ substituents closer to the *meso*-carbon of the BODIPY unit, are red-shifted compared to M1–M3, indicating the electronic communication between BODIPY and the attached TAB unit. In contrast, a blue shift was observed in **3**, **4**, and **6**, which have –CH₃ substituents closer to the *meso*-carbon of the BODIPY unit. A robust blue shift was observed in **4**, which has a sterically demanding duryl spacer. Furthermore, there were no additional bands corresponding to the electronic transitions of the different mixed electronic levels of the molecular partners, as observed for thiophene-substituted boryl-BODIPY triads reported elsewhere.⁷

Based on these results, the higher energy bands in the region from 300 to 400 nm can be attributed to the $\pi \rightarrow \pi^*$ and $\pi \rightarrow \pi_{(B)}^*$ transition of the TAB moiety, and the intense band at a lower energy (~520 nm) could be arise from the HOMO to LUMO transition centered in the BODIPY moiety. The TD-DFT results indicated two major electronic transitions in all the compounds (Table S8 and S9), the HOMO \rightarrow LUMO transition centered on the BODIPY unit and the HOMO – 1 \rightarrow LUMO + 1 transition centered on the TAB moiety. The absorption spectral features of these dyads revealed that TAB and BODIPY could be combined to form dyads in such a manner that the molecular partners retain the characteristics of their electronic levels to a large extent. Further, an important fact of this investigation on the intramolecular energy transfer is that the selective excitation of the TAB group in the region of ~300–350 nm is possible for all dyads.

Normalized emission spectra of **1–6** with R1 and R2 are depicted in Figure 3, and all the photophysical data are summarized in Table 2. Upon excitation at 350 nm, **1**, **2**, and **5** showed two emission bands at ~410 and ~520 nm, respectively; however, the BODIPY-centered band at 520 nm is slightly broader than the PL band observed for model compounds M1–M3 (Figure 3). Compounds **3**, **4**, and **6** with two methyl groups adjacent to the BODIPY *meso*-carbon also exhibit dual PL bands at ~410 and ~520 nm, respectively,

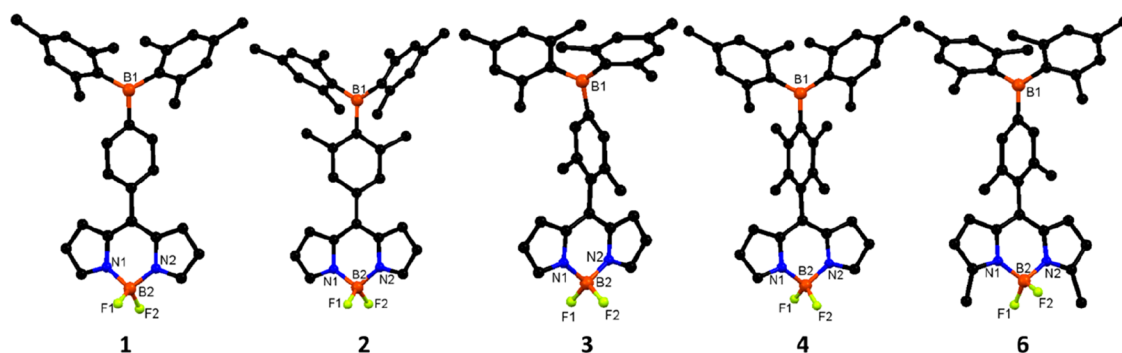


Figure 2. Molecular structures of 1–6. All the hydrogens are omitted for clarity.

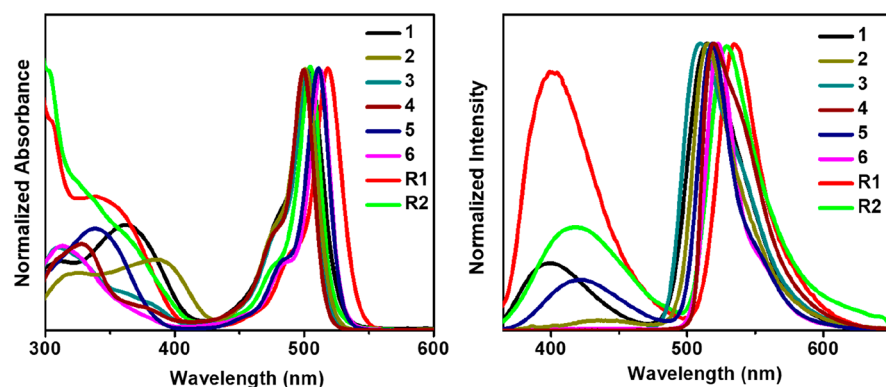
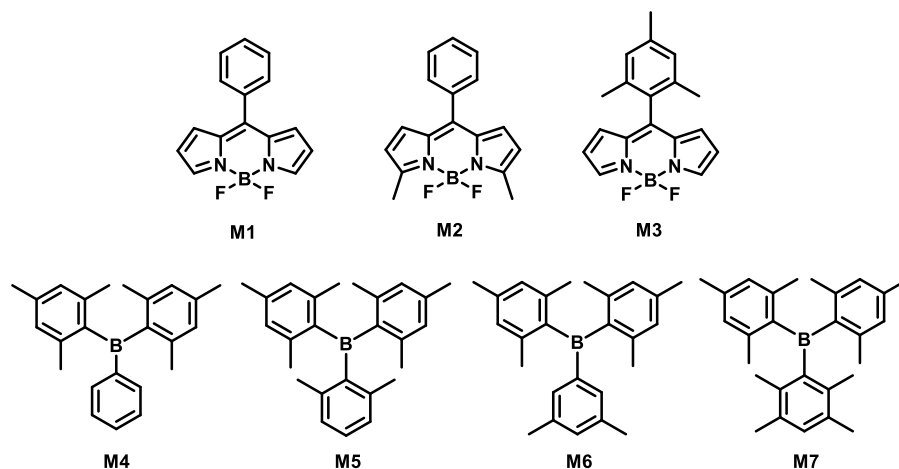


Figure 3. Normalized absorption (left) and emission (right) spectra of 1–6, R1, and R2 in dichloromethane (concentration of $10 \mu\text{M}$, λ_{ex} at 350 nm).

Chart 2. Chemical Structures of the Model Compounds (M1–M7)



under similar conditions. The width of the lower-energy band for all the molecules is comparable to those of the bands observed in M1–M3; in sharp contrast, the ~ 410 nm PL band in 3, 4, and 6 was noticeably weaker than the band observed in 1 (spacer devoid of $-\text{CH}_3$ substituents), 2, and 5 (with two methyl groups adjacent to the $\text{Mes}_2\text{B}-$ unit). Compound R2 has two methyl groups on the BODIPY moiety adjacent to the *meso*-carbon and show PL features comparable to those of 1, 2, and 5 that significantly differ from those of 3, 4, and 6. In contrast, R1 is devoid of substituents on both the phenyl spacer, and the first and seventh positions of the BODIPY moiety show dual emissions with equal intensities. These results strongly suggested that the position of the methyl

groups in the spacer plays a vital role in controlling the energy transfer from TAB to the BODIPY moiety.

From the PL spectra of 1–6, it is clear that the emitting S1 state is primarily localized on the BODIPY moiety. The weak bathochromic shift and line broadening of the BODIPY fluorescence band can be attributed to the weak electronic coupling between the TAB and BODIPY moieties. The presence of emission from the TAB chromophore in these dyads points to the fact that the segmental features found in their ground state have prevailed in the excited state. Evidently, the weak coupling between the TAB and BODIPY and the rigidity imposed by additional methyl groups on the aryl spacer in 3, 4, and 6 facilitate faster energy transfer than the excited-

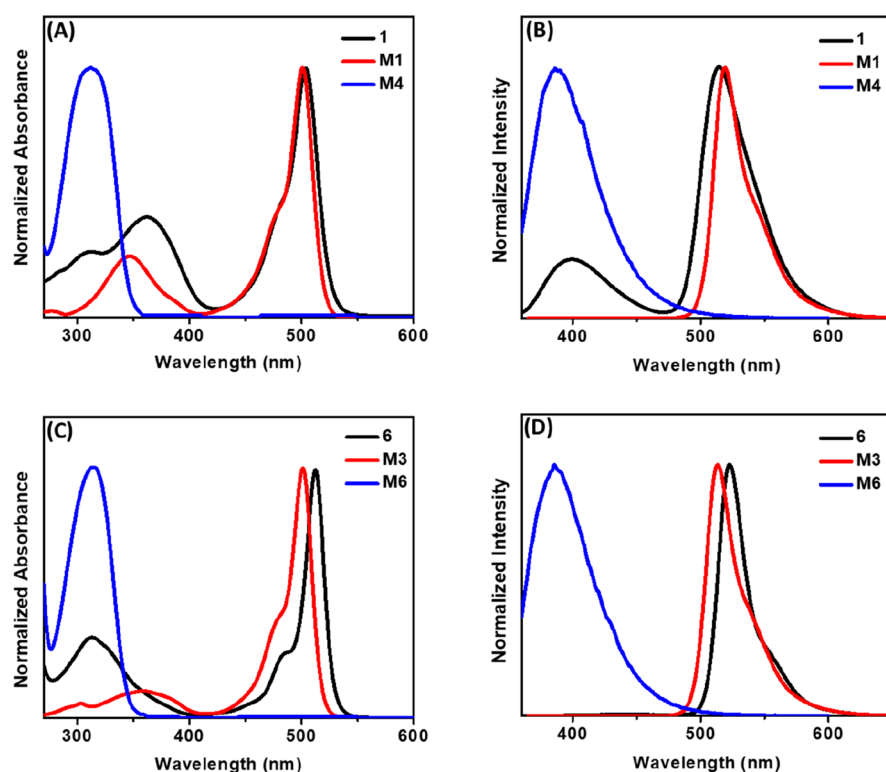


Figure 4. Normalized absorption and emission spectra of **1**, **6**, and the respective model compounds **M1**, **M3**, **M4**, and **M6** in DCM (λ_{ex} at 350 nm, concentration of 10 μM).

Table 2. Absorption Band Maxima ($\lambda_{\text{abs}}^{\text{max}}$, nm) with Molar Extinction Coefficients (ϵ) and Fluorescence Maxima ($\lambda_{\text{em}}^{\text{max}}$, nm) of Dyads (In Dichloromethane, 10 μM Concentration)

compound	λ_{abs} (nm)	ϵ ($\text{M}^{-1} \text{cm}^{-1}$)	λ_{em} (nm)	Stokes shift (cm^{-1})	Φ^a
1	359, 504	5.67×10^4 , 1.02×10^5	418, 523	5263	0.38
2	387, 500	1.12×10^4 , 4.43×10^4	445, 514	7143	0.34
3	309, 502	1.71×10^4 , 5.39×10^4	514	8333	0.81
4	323, 499	1.25×10^4 , 3.88×10^4	511	8333	0.84
5	338, 510	1.98×10^4 , 5.07×10^4	425, 524	7143	0.76
6	313, 512	1.18×10^4 , 5.31×10^4	523	9091	0.86
R1	355, 512	2.51×10^4 , 7.21×10^4	410, 531	4762	0.49
R2	350, 501	2.49×10^4 , 8.87×10^4	405, 515	7143	0.42

^aThe PL quantum yields were calculated for the dichloromethane solution using the following equation: $\Phi = \Phi_{\text{R}} \times (I/I_{\text{R}}) \times (A_{\text{R}}/A) \times (\eta^2/\eta_{\text{R}}^2)$, here Φ is the quantum yield, I is the area under the PL band, A is the absorbance at λ_{ex} , and η is the refractive index of the solvent. Standard 0.1 M H_2SO_4 quinine sulfate ($\Phi_{\text{R}} = 0.577$) was used. The emission wavelength used was $\lambda_{\text{ex}} = 350$ nm.

state molecular rearrangements. Interestingly, although the electronic coupling between the D and A moieties in **1**, **2**, and **5** is larger than in those in **3**, **4**, and **6**, the excited state molecular conformational changes occur faster than the energy transfer process because of molecular flexibility; consequently, well-separated dual-emission peaks were observed. TD-DFT-computed electronic transitions revealed that electronic transitions in **1**, **2**, and **5** involving the LUMO have a contribution from the vacant p -orbital of tricoordinate boron; in contrast, such a contribution is missing in **3**, **4**, and **6**. As a result, **1**, **2**, and **5** show emissions in the boron region, which are nearly absent in **3**, **4**, and **6**.

Concentration-dependent absorption and emission spectra of all the molecules were recorded in different concentrations (10^{-5} and 10^{-6} M, Figures S61 and S62, respectively). When the compound concentration decreased, the intensity of absorption and emission bands decreased without a shift in peak maxima. The ratio of both the emission bands in **1–6**

remains constant in all concentrations. Excitation spectra of all the compounds were recorded by monitoring the decay of the corresponding PL bands. Aside from compounds **1** and **5**, all the other compounds excitation spectra are similar to their respective compound's absorption spectra (Figure S65). The difference in the excitation and absorption spectra of **1** and **5** can be attributed to the difference in their ground- and excited-state structures. The solvent polarity-dependent absorbance and PL of all the compounds were studied in detail. The results indicated that the emissive states in these compounds are dominated by nonpolar excited states (Figures S57 and S58), which is also supported by the calculated excited-state dipole moment values (Table S6).

Model compounds **M1–M3** showed a single PL band corresponding to the BODIPY unit, whereas **M4–M7** showed a band at 390 nm. The larger energy gap ($\sim 5557 \text{ cm}^{-1}$) between these two bands in **1–6** suggests that the emissions come from different electronic states, i.e., Franck–Condon

(FC) excited states (the molecular identity is preserved) and a relaxed S_1 state (energy-transfer state, see below). It has been well-established that a substantial overlap between the emission spectrum of the donor and the absorption spectrum of the acceptor invites Förster resonance energy transfer (FRET) between the donor and the acceptor (Figure 5). Upon

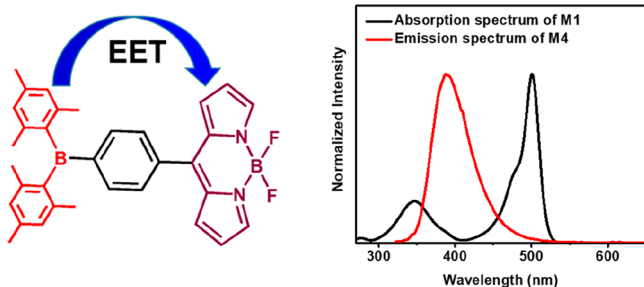


Figure 5. (Left) Schematic representation of the excitation energy transfer from the donor (TAB) to the acceptor (BODIPY). (Right) Comparison of the emission spectrum of TAB (M1) and the absorption spectrum of BODIPY (M4).

excitation, the molecule reaches the FC state where within the time window the energy transfer takes place from D to A, going to a relaxed S_1 state. Furthermore, favorable orientations of the donor–acceptor chromophores, the closeness between the donor and the acceptor, and the nonmixing FMOs of two chromophores are salient criteria for FRET process. All the requirements mentioned above were fulfilled in dyads 1–6; thus, FRET is operative in these dyes. Therefore, dual emission in these dyads is due to the simultaneous emission from the FC state (boryl emission) and the energy-transfer state (FRET emission). The difference in the ratio of the dual-emission bands in these compounds indicated that the EET operates differently in these compounds depending on the molecular conformations.

Feeble luminescence from TAB components indicated that the energy transfer from TAB to BODIPY is very efficient in these dyads. The energy-transfer efficiencies (ETEs)^{63–65} in 1–6 were calculated from their respective PL spectra using the equation $ETE = \frac{A-D}{A}$, where D is the emission intensity of the donor TAB and A is the emission intensity of the acceptor BODIPY dye. Higher ETEs were calculated for 2, 3, 4, 5, and 6, which have additional methyl substituents on the aryl spacer either close to the *meso*-carbon or the Mes2B- moiety, than for 1, R1 and R2, which are devoid of substituents on the phenyl spacer. These results indicated that the identity of the spacer connecting the donor and the acceptor is crucial in altering the EET and PL quantum yield in these types of compounds. The energy-transfer rates for 1, 2, 5, R1, and R2 were calculated (see the Supporting Information for details, eq S1), and the results are summarized in Table 3.⁶⁶ The calculated energy-transfer rate amply corroborated the ETE, as the compounds with higher ETEs show higher energy-transfer rates and vice versa.

Time-resolved decay kinetics were performed on all the compounds (Figure S67–S82) in dichloromethane, and the results are summarized in Table S3. In all the compounds, the higher-energy band at ~410 nm showed a biexponential decay with a short and a long lifetime. The lower-energy band at ~510 nm showed a single exponential decay for 3, 4, and 5 like in R1 and R2, while a biexponential decay was obtained for 1,

Table 3. TAB → BODIPY Energy-Transfer Efficiency (ETE) in 1–6, R1, and R2 and the Corresponding Energy-Transfer Rate

compounds	1	2	3	4	5	6	R1	R2
ETE (%)	54	95	100	100	81	100	16	78
ETE rate (10^7 s^{-1})	53	1293			290		9	161

2, and 6 (Table S3). The lifetime of all the compounds was in the nanosecond range, indicating that the emissions are from a singlet excited state. The longer lifetimes (ca. ~6 to 8 ns) in 3, 4, 5, and 6 indicate that nonradiative decay in these compounds with a rigid structure is lower than for other compounds with a flexible molecular structure. These results are also consistent with the PL quantum yields of 1–6.

The PL quantum yield (PLQY), radiative rate, and nonradiative rate constants were also calculated (Table S3) for all the dyads. The PLQYs of 3, 4, 5, and 6 are higher (almost double) than those obtained for 1, 2, R1, and R2. A higher quantum yield and a longer lifetime for longer wavelength bands suggest that the energy transfer is more efficient in compounds 3, 4, 5, and 6. On the other hand, the results obtained for 1, 2, R1, and R2 suggested that energy transfer is less efficient in these systems. From these results, one can conclude that all the newly synthesized compounds show dual-emission characteristics because of incomplete fluorescence resonance energy transfer from the donor to acceptor moieties.

Cyclic Voltammetry Studies. Cyclic voltammetry studies were performed for 1–6 and R1 and R2 to gain a detailed insight of their electronic structures (Figures S94 and S95 and Table S7). The experiments were performed in a dichloromethane solution (1 mM) for oxidation and in a THF solution (1 mM) for reduction with TBAPF₆ (100 mM) as the supporting electrolyte at 20 °C using a Pt disk as a working electrode, a Pt wire as a counter electrode, and a Ag wire as a reference electrode. The potential scales are referenced to the ferrocene/ferrocenium couple. During the anodic scan, only 6 and R2 showed single reversible oxidation processes at 0.91 and 0.80 V, respectively. All other molecules show single reversible oxidation processes in the region from 1.20 to 1.25 V, which is very similar to the reported data for M1 (1.19 V).⁶⁷ The lower values for 6 and R2 could be due to the electron-donating effect of the extra methyl groups present in the molecules. During the cathodic scan, all the molecules show two reduction processes. Reversible reduction processes were observed in the range from –1.2 to –1.6 V. 1 has the lowest first-reduction potential at –1.18 V, which is comparable to the reported value –1.15 V for M1,⁶⁷ whereas 6 has the highest value of –1.64 V. As 5, 6, and R2 have extra methyl groups on the bodipy core, they have higher reduction potentials compared to those of the others. Although R1 has the extra methyl groups on the BODIPY core, the effect of the TAB group probably accounts for the reduction potential at –1.34 V. The second reduction potential was observed from –1.8 to –2.5 V. This is also minimum for 1 (–1.79 V) and a maximum for 6 (–2.48 V). Reduction peaks corresponding to the triarylboron center would be ca. –2.5 V,⁶⁸ although they were not observed for these molecules even when the scans were done up to –3.5 V (with respect to Fc/Fc⁺). HOMO and LUMO energies were also calculated using the first-oxidation and first-reduction potentials and were comparable to the

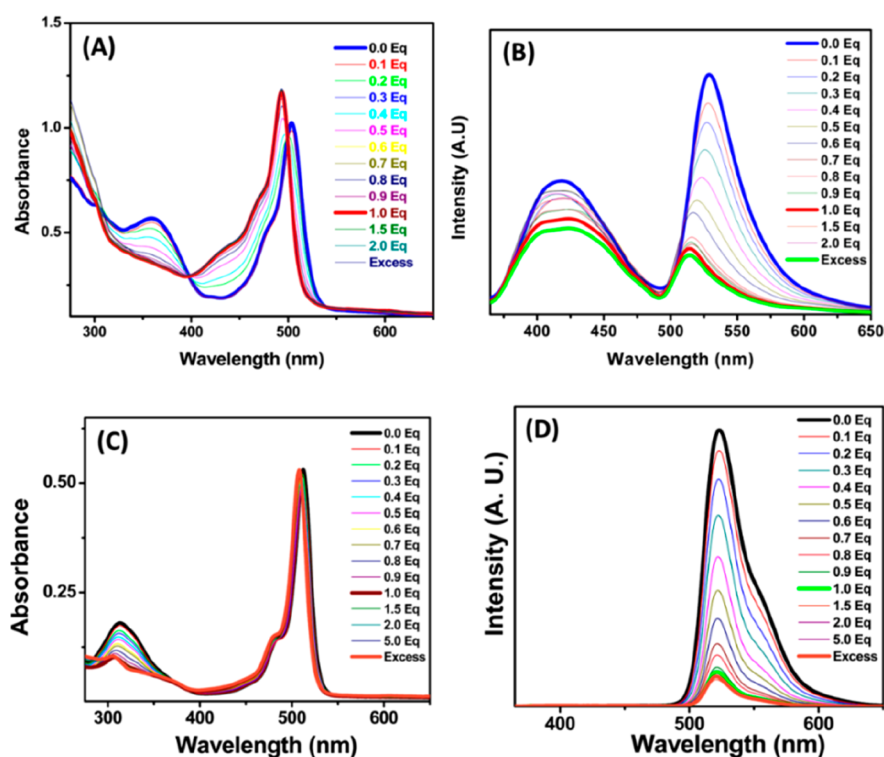


Figure 6. Changes in absorption and emission spectra of **1** and **6** (in DCM, 1.0×10^{-5} M) upon the incremental addition of TBAF (in DCM, 1.0×10^{-3} M). (A) Absorption of **1**, (B) emission of **1**, (C) absorption of **6**, and (D) emission of **6** ($\lambda_{\text{ex}} = 350$ nm).

energies obtained from DFT calculations, as depicted in Table S7.

Effect of External Chemical Stimuli on EET in 1–6. As discussed, *vide supra*, the boron center in the TAB moiety can expand its coordination from three to four in the presence of a suitable anion and consequently modify the EET from TAB to the BODIPY moiety. Thus, anion binding studies on dyads **1–6** were carried out in detail to understand the effect of molecular conformation on the sensing and EET from the donor (TAB) to the acceptor (BODIPY). Upon fluoride addition, the absorption bands in **1**, **3**, and **6** were blue-shifted with an isosbestic point, indicating that the fluoride binding disrupts the electronic conjugation between the TAB and BODIPY moieties through an empty p-orbital on boron in the TAB fragments (Figures 6 and S84). The optical changes were more apparent in **1** than in **3** and **6**, with a methyl group close to the *meso*-carbon of the BODIPY unit. Compounds **2**, **4**, and **5** with sterically hindered tricoordinate boron (an aryl spacer with methyl groups around the Mes_2B moiety) do not show appreciable changes in their absorption spectra in the presence of fluoride, indicating that the steric crowding around TAB significantly affects the fluoride binding in these compounds. These observations are comparable to the fluoride binding results of TABs reported elsewhere.^{7,59} The fluoride binding events in these compounds were also studied using ^{19}F NMR spectroscopic methods (Figures S86–S88 for **1**, **3**, and **6**, respectively). In the presence of fluoride, compounds **1**, **3**, and **6** showed a ^{19}F signal corresponding to the $(\text{Ar})_3\text{BF}$ moiety at ca. -172 ppm. In contrast, compounds **2**, **4**, and **5** did not show a ^{19}F signal corresponding to the $(\text{Ar})_3\text{BF}$ moiety. These results indicated that the fluoride ions bind to the less sterically hindered tricoordinate boron in **1**, **3**, and **6** and not to the sterically demanding tricoordinate boron in **2**, **4**, and **5**. This

observation directly corroborates the results obtained in optical studies.

Fluoride binding strongly quenched the PL of **1**, **3**, and **6**; however, very minimal PL quenching was observed in **2**, **4**, and **5** (Figures 6 and S84). This result indicated that fluoride binding altered the energy transfer from the donor (TAB) to the acceptor (BODIPY) moiety. Interestingly, with the successive addition of fluoride ions, the intensities of both the emission bands in **1** gradually decreased (Figure 6). However, a rapid decrease in the intensity of the longer-wavelength band compared to that of the lower-wavelength band was observed for **6**. It was found that the addition of fluoride ions did not quench the BODIPY emission in **M1**, **M3**, and the boryl emission of **M8** (boron is much more sterically protected) (Chart S1 and Figure S91). However, F^- binding altered the absorption and extinguished the boryl emission in **M4** (boron is less sterically protected). The fluorescence excitation spectra ($\lambda_{\text{em}} = 520$ nm) of **1**, **3**, and **6** were recorded in the presence of TBAF (Figure S85). In accordance with the quenching of the BODIPY emission band in the presence of fluoride, the intensities of both the excitation bands also decreased. Thus, the absence of BODIPY emission in fluoride-bound adducts of **1**, **3**, and **6** upon being excited at the TAB domain indicates a decrease in the energy transfer from TAB \rightarrow BODIPY.

Like fluoride, TABs bind equally to cyanide and show different optical features. The addition of a cyanide ion brings about significantly fewer changes in the optical characteristics of **1**, **3**, and **6** and no changes in cases of **2**, **4**, and **5** (Figure S89). Furthermore, the optical feature of **1–6** did not change in the presence of Cl^- , Br^- , I^- , ClO_4^- , HSO_4^- , H_2PO_4^- , NO_3^- , and PF_6^- (10 equiv or excess) (Figure S90), indicating that these probes are selective to only fluoride ions. The limits of detection (LOD) for **1**, **3**, and **6** were calculated to be 1.34

(± 0.06), 1.00 (± 0.05), and 0.07 (± 0.03) ppm, respectively. These results are comparable with the values reported elsewhere for similar TAB compounds.

Finally, the reversibility of fluoride binding in **1**, **3**, and **6** was studied using $\text{BF}_3 \cdot \text{Et}_2\text{O}$ as an external Lewis acid (Figure S94). The addition of $\text{BF}_3 \cdot \text{Et}_2\text{O}$ to the solutions of **1** + F^- , **3** + F^- , and **6** + F^- , restored the PL features of the free Lewis acids (**1**, **3**, and **6**), indicating that $\text{BF}_3 \cdot \text{Et}_2\text{O}$ abstracted the boron-bound fluoride in these compounds and subsequently regenerated **1**, **3**, and **6**. Thus, these TAB-BODIPY dyads can also be used for ON/OFF and OFF/OFF fluorescence switching in the presence and absence of fluoride ions, respectively.

CONCLUSION

We have demonstrated a versatile design strategy for developing a new class of dual-emissive dyads. Dyads **1–6** were constructed with similar molecular building blocks, and their molecular conformations were systematically fine-tuned by judiciously varying the number of methyl substituents on both TAB and BODIPY moieties. Despite the direct attachment of TAB to the BODIPY moiety, the electronic interactions are weak, and the absorption bands corresponding to individual molecular subunits can be recognized in the spectra of the dyads. The covalent linking of TAB unit at the *meso*-carbon of BODIPY does not affect the ground and Franck–Condon excited states of the individual chromophores. Furthermore, a weak coupling between TAB and BODIPY accounts for the slight red-shift and broadening of the BODIPY fluorescence band. The residual TAB emission in these dyads points to the fact that the segmental features found in their ground state prevail in the excited state. The weak coupling between TAB and BODIPY combined with the steric hindrance imposed by methyl groups on the aryl spacer in **3**, **4**, and **6** enables faster energy transfer than the excited-state molecular reorganization. Though the electronic coupling between the donor and acceptor moieties in **1**, **2**, and **5** is significantly larger than that in **3**, **4**, and **6**, the excited-state molecular reorganization occurs faster than the energy transfer because the molecular flexibility in the latter set of dyads leads to intriguing dual-emission features. This study revealed that TAB and BODIPY may be combined to form dyads in such a manner that the molecular partners retain their characteristic electronic levels to a large extent. An important fact of this investigation on intramolecular energy transfer is that the selective excitation of the TAB group in the region $\sim 300\text{--}350$ nm is possible for all dyads. Further, external stimuli, such as fluoride, can be used as probes to understand the EET in these dyads.

ASSOCIATED CONTENT

Supporting Information

The Supporting Information is available free of charge at <https://pubs.acs.org/doi/10.1021/acs.inorgchem.0c02739>.

Detailed synthesis procedure, characterization data, additional photophysical studies, NMR studies, and theoretical calculation data (PDF)

Accession Codes

CCDC 1994506–1994510 contain the supplementary crystallographic data for this paper. These data can be obtained free of charge via www.ccdc.cam.ac.uk/data_request/cif, or by emailing data_request@ccdc.cam.ac.uk, or by contacting The

Cambridge Crystallographic Data Centre, 12 Union Road, Cambridge CB2 1EZ, UK; fax: +44 1223 336033.

AUTHOR INFORMATION

Corresponding Authors

Pakkirisamy Thilagar – Department of Inorganic and Physical Chemistry, Indian Institute of Science, Bangalore 560012, India; orcid.org/0000-0001-9569-7733; Email: thilagar@iisc.ac.in

Chinna Ayya Swamy P – Department of Chemistry, National Institute of Technology Calicut, Kozhikode 673601, India; orcid.org/0000-0001-7875-9517; Email: swamy@nitc.ac.in

Authors

Rajendra Prasad Nandi – Department of Inorganic and Physical Chemistry, Indian Institute of Science, Bangalore 560012, India; orcid.org/0000-0001-9597-9466

Pandi Dhanalakshmi – Department of Inorganic and Physical Chemistry, Indian Institute of Science, Bangalore 560012, India

Santosh Kumar Behera – Department of Inorganic and Physical Chemistry, Indian Institute of Science, Bangalore 560012, India; orcid.org/0000-0003-2066-4712

Complete contact information is available at:

<https://pubs.acs.org/10.1021/acs.inorgchem.0c02739>

Funding

SERB, New Delhi, India. File no. EMR/2015/000572 dtd. 21.3.16

Notes

The authors declare no competing financial interest.

ACKNOWLEDGMENTS

P.T. thanks SERB New Delhi, India for financial support; C.A.S.P. and R.P.N. thank IISc for a research fellowship; S.K.B. thanks UGC, New Delhi, India for a Kothari postdoctoral fellowship; and P.D. thanks SERB for a National Postdoctoral fellowship (file no. PDF/2018/000099) New Delhi, India. Authors thank the IPC Department and IISc Bangalore, India for infrastructure and instrumental facilities.

REFERENCES

- (1) Friend, R. H.; Gymer, R. W.; Holmes, A. B.; Burroughes, J. H.; Marks, R. N.; Taliani, C.; Bradley, D. D. C.; Santos, D. A. D.; Bredas, J. L.; Logdlund, M.; Salaneck, W. R. Electroluminescence in conjugated polymers. *Nature* **1999**, *397*, 121–128.
- (2) *Organic Light-Emitting Devices*; Shinar, J., Ed.; Springer-Verlag: New York: New York, NY, 2004.
- (3) Goncalves, M. S. Fluorescent labeling of biomolecules with organic probes. *Chem. Rev.* **2009**, *109*, 190–212.
- (4) Ding, D.; Li, K.; Liu, B.; Tang, B. Z. Bioprobes based on AIE fluorogens. *Acc. Chem. Res.* **2013**, *46*, 2441–53.
- (5) Liu, Y.; Pan, M.; Yang, Q.-Y.; Fu, L.; Li, K.; Wei, S.-C.; Su, C.-Y. Dual-Emission from a Single-Phase Eu-Ag Metal-Organic Framework: An Alternative Way to Get White-Light Phosphor. *Chem. Mater.* **2012**, *24*, 1954–1960.
- (6) P, P. C. S.; Mukherjee, S.; Thilagar, P. Multichannel-emissive V-shaped boryl-BODIPY dyads: Synthesis, structure, and remarkably diverse response toward fluoride. *Inorg. Chem.* **2014**, *53*, 4813–4823.
- (7) Sarkar, S. K.; Thilagar, P. A borane-bithiophene-BODIPY triad: intriguing tricolor emission and selective fluorescence response towards fluoride ions. *Chem. Commun.* **2013**, *49*, 8558–60.

- (8) Zhou, C.; Zhang, S.; Gao, Y.; Liu, H.; Shan, T.; Liang, X.; Yang, B.; Ma, Y. Ternary Emission of Fluorescence and Dual Phosphorescence at Room Temperature: A Single-Molecule White Light Emitter Based on Pure Organic Aza-Aromatic Material. *Adv. Funct. Mater.* **2018**, *28*, 1802407.
- (9) He, Z. K.; Zhao, W. J.; Lam, J. W. Y.; Peng, Q.; Ma, H. L.; Liang, G. D.; Shuai, Z. G.; Tang, B. White light emission from a single organic molecule with dual phosphorescence at room temperature. *Nat. Commun.* **2017**, *8*, 416.
- (10) Yang, J.; Ren, Z.; Xie, Z.; Liu, Y.; Wang, C.; Xie, Y.; Peng, Q.; Xu, B.; Tian, W.; Zhang, F.; et al. AIEgen with fluorescence-phosphorescence dual mechanoluminescence at room temperature. *Angew. Chem., Int. Ed.* **2017**, *56*, 880–884.
- (11) Zhang, G.; Palmer, G. M.; Dewhurst, M. W.; Fraser, C. L. A dual-emissive-materials design concept enables tumour hypoxia imaging. *Nat. Mater.* **2009**, *8*, 747–51.
- (12) Gong, Y.; Zhao, L.; Peng, Q.; Fan, D.; Yuan, W. Z.; Zhang, Y.; Tang, B. Z. Crystallization-induced dual emission from metal- and heavy atom-free aromatic acids and esters. *Chem. Sci.* **2015**, *6*, 4438–4444.
- (13) Li, X.; Baryshnikov, G.; Deng, C.; Bao, X.; Wu, B.; Zhou, Y.; Agren, H.; Zhu, L. A three-dimensional ratiometric sensing strategy on unimolecular fluorescence-thermally activated delayed fluorescence dual emission. *Nat. Commun.* **2019**, *10*, 731.
- (14) Takeda, Y.; Kaihara, T.; Okazaki, M.; Higginbotham, H.; Data, P.; Tohnai, N.; Minakata, S. Conformationally-flexible and moderately electron-donating units-installed D-A-D triad enabling multicolor-changing mechanochromic luminescence, TADF and room-temperature phosphorescence. *Chem. Commun.* **2018**, *54*, 6847–6850.
- (15) Bhattacharjee, I.; Acharya, N.; Bhatia, H.; Ray, D. Dual Emission through Thermally Activated Delayed Fluorescence and Room-Temperature Phosphorescence, and Their Thermal Enhancement via Solid-State Structural Change in a Carbazole-Quinoline Conjugate. *J. Phys. Chem. Lett.* **2018**, *9*, 2733–2738.
- (16) Chen, C. J.; Huang, R. J.; Batsanov, A. S.; Pander, P.; Hsu, Y. T.; Chi, Z. G.; Dias, F. B.; Bryce, M. R. Intramolecular Charge Transfer Controls Switching Between Room Temperature Phosphorescence and Thermally Activated Delayed Fluorescence. *Angew. Chem., Int. Ed.* **2018**, *57*, 16407–16411.
- (17) Cho, Y. J.; Jeon, S. K.; Chin, B. D.; Yu, E.; Lee, J. Y. The design of dual emitting cores for green thermally activated delayed fluorescent materials. *Angew. Chem., Int. Ed.* **2015**, *54*, 5201–4.
- (18) Lippert, E.; Lüder, W.; Moll, F.; Nägele, W.; Boos, H.; Prigge, H.; Seibold-Blankenstein, I. Conversion of electron excitation energy. *Angew. Chem.* **1961**, *73*, 695–706.
- (19) Zachariasse, K. A.; Grobys, M.; vanderHaar, T.; Hebecker, A.; Il'ichev, Y. V.; Jiang, Y. B.; Morawski, O.; Kuhnle, W. Intramolecular charge transfer in the excited state. Kinetics and configurational changes. *J. Photochem. Photobiol., A* **1996**, *102*, 59–70.
- (20) Rotkiewicz, K.; Grellmann, K.; Grabowski, Z. Reinterpretation of the anomalous fluorescence of pn, n-dimethylamino-benzonitrile. *Chem. Phys. Lett.* **1973**, *19*, 315–318.
- (21) Siemiarz, A.; Grabowski, Z. R.; Krówczynski, A.; Asher, M.; Ottolenghi, M. Two emitting states of excited p-(9-anthryl)-n, n-dimethylaniline derivatives in polar solvents. *Chem. Phys. Lett.* **1977**, *51*, 315–320.
- (22) Grabowski, Z. R.; Rotkiewicz, K.; Siemiarz, A. Dual fluorescence of donor-acceptor molecules and the Twisted Intramolecular Charge Transfer (TICT) states. *J. Lumin.* **1979**, *18–19*, 420–424.
- (23) Kasha, M. Proton-Transfer Spectroscopy - Perturbation of the Tautomerization Potential. *J. Chem. Soc., Faraday Trans. 2* **1986**, *82*, 2379–2392.
- (24) Formosinho, S. J.; Arnaut, L. G. Excited-state proton transfer reactions II. Intramolecular reactions. *J. Photochem. Photobiol., A* **1993**, *75*, 21–48.
- (25) Zhao, J.; Ji, S.; Chen, Y.; Guo, H.; Yang, P. Excited state intramolecular proton transfer (ESIPT): from principal photophysics to the development of new chromophores and applications in fluorescent molecular probes and luminescent materials. *Phys. Chem. Chem. Phys.* **2012**, *14*, 8803–17.
- (26) Dexter, D. L. A Theory of Sensitized Luminescence in Solids. *J. Chem. Phys.* **1953**, *21*, 836–850.
- (27) Forster, T. 10th Spiers Memorial Lecture - Transfer Mechanisms of Electronic Excitation. *Discuss. Faraday Soc.* **1959**, *27*, 7–17.
- (28) Scandola, F.; Balzani, V. Energy-transfer processes of excited states of coordination compounds. *J. Chem. Educ.* **1983**, *60* (10), 814.
- (29) Valeur, B. *Molecular Fluorescence: Principles and Applications*; Wiley-VCH Verlag GmbH: Weinheim, Germany, 2001.
- (30) Wang, J.; Huang, J.; Du, L.; Lan, Z. Photoinduced Ultrafast Intramolecular Excited-State Energy Transfer in the Silylene-Bridged Biphenyl and Stilbene (SBS) System: A Nonadiabatic Dynamics Point of View. *J. Phys. Chem. A* **2015**, *119*, 6937–48.
- (31) Zhao, W.; Cheung, T. S.; Jiang, N.; Huang, W.; Lam, J. W. Y.; Zhang, X.; He, Z.; Tang, B. Z. Boosting the efficiency of organic persistent room-temperature phosphorescence by intramolecular triplet-triplet energy transfer. *Nat. Commun.* **2019**, *10*, 1595.
- (32) Cravcenco, A.; Hertzog, M.; Ye, C.; Iqbal, M. N.; Mueller, U.; Eriksson, L.; Borjesson, K. Multiplicity conversion based on intramolecular triplet-to-singlet energy transfer. *Sci. Adv.* **2019**, *5*, No. eaaw5978.
- (33) Selvin, P. R. The renaissance of fluorescence resonance energy transfer. *Nat. Struct. Biol.* **2000**, *7*, 730–4.
- (34) Stryer, L.; Haugland, R. P. Energy transfer: a spectroscopic ruler. *Proc. Natl. Acad. Sci. U. S. A.* **1967**, *58*, 719–26.
- (35) Clegg, R. M. Fluorescence resonance energy transfer. *Curr. Opin. Biotechnol.* **1995**, *6*, 103–10.
- (36) Takakusa, H.; Kikuchi, K.; Urano, Y.; Sakamoto, S.; Yamaguchi, K.; Nagano, T. Design and synthesis of an enzyme-cleavable sensor molecule for phosphodiesterase activity based on fluorescence resonance energy transfer. *J. Am. Chem. Soc.* **2002**, *124*, 1653–7.
- (37) Albers, A. E.; Okreglak, V. S.; Chang, C. J. A FRET-based approach to ratiometric fluorescence detection of hydrogen peroxide. *J. Am. Chem. Soc.* **2006**, *128*, 9640–1.
- (38) Han, Z. X.; Zhang, X. B.; Li, Z.; Gong, Y. J.; Wu, X. Y.; Jin, Z.; He, C. M.; Jian, L. X.; Zhang, J.; Shen, G. L.; Yu, R. Q. Efficient fluorescence resonance energy transfer-based ratiometric fluorescent cellular imaging probe for Zn(2+) using a rhodamine spirolactam as a trigger. *Anal. Chem.* **2010**, *82*, 3108–13.
- (39) Zhang, X.; Xiao, Y.; Qian, X. A ratiometric fluorescent probe based on FRET for imaging Hg²⁺ ions in living cells. *Angew. Chem., Int. Ed.* **2008**, *47*, 8025–9.
- (40) Guliyev, R.; Coskun, A.; Akkaya, E. U. Design strategies for ratiometric chemosensors: modulation of excitation energy transfer at the energy donor site. *J. Am. Chem. Soc.* **2009**, *131*, 9007–13.
- (41) Laquai, F.; Park, Y. S.; Kim, J. J.; Basche, T. Excitation energy transfer in organic materials: from fundamentals to optoelectronic devices. *Macromol. Rapid Commun.* **2009**, *30*, 1203–31.
- (42) Hardin, B. E.; Sellinger, A.; Moehl, T.; Humphry-Baker, R.; Moser, J. E.; Wang, P.; Zakeeruddin, S. M.; Gratzel, M.; McGehee, M. D. Energy and hole transfer between dyes attached to titania in cosensitized dye-sensitized solar cells. *J. Am. Chem. Soc.* **2011**, *133*, 10662–7.
- (43) Zhang, D.; Cai, M.; Zhang, Y.; Bin, Z.; Zhang, D.; Duan, L. Simultaneous Enhancement of Efficiency and Stability of Phosphorescent OLEDs Based on Efficient Forster Energy Transfer from Interface Exciplex. *ACS Appl. Mater. Interfaces* **2016**, *8*, 3825–32.
- (44) Yamaguchi, S.; Akiyama, S.; Tamao, K. Colorimetric fluoride ion sensing by boron-containing pi-electron systems. *J. Am. Chem. Soc.* **2001**, *123*, 11372–5.
- (45) Sudhakar, P.; Neena, K. K.; Thilagar, P. Borylated perylene diimide: self-assembly, photophysics and sensing application. *Dalton Trans.* **2019**, *48*, 7218–7226.
- (46) Boens, N.; Leen, V.; Dehaen, W. Fluorescent indicators based on BODIPY. *Chem. Soc. Rev.* **2012**, *41*, 1130–72.

- (47) Loudet, A.; Burgess, K. BODIPY dyes and their derivatives: syntheses and spectroscopic properties. *Chem. Rev.* **2007**, *107*, 4891–932.
- (48) Ulrich, G.; Ziesel, R.; Harriman, A. The chemistry of fluorescent bodipy dyes: versatility unsurpassed. *Angew. Chem., Int. Ed.* **2008**, *47*, 1184–201.
- (49) Filatov, M. A. Heavy-atom-free BODIPY photosensitizers with intersystem crossing mediated by intramolecular photoinduced electron transfer. *Org. Biomol. Chem.* **2020**, *18*, 10–27.
- (50) Lu, J. S.; Ko, S. B.; Walters, N. R.; Wang, S. Decorating BODIPY with three- and four-coordinate boron groups. *Org. Lett.* **2012**, *14*, 5660–3.
- (51) Huh, J. O.; Do, Y.; Lee, M. H. A BODIPY-Borane Dyad for the Selective Complexation of Cyanide Ion. *Organometallics* **2008**, *27*, 1022–1025.
- (52) Fu, G. L.; Pan, H.; Zhao, Y. H.; Zhao, C. H. Solid-state emissive triarylborane-based BODIPY dyes: photophysical properties and fluorescent sensing for fluoride and cyanide ions. *Org. Biomol. Chem.* **2011**, *9*, 8141–6.
- (53) Sun, H. B.; Dong, X. C.; Liu, S. J.; Zhao, Q.; Mou, X.; Yang, H. Y.; Huang, W. Excellent BODIPY Dye Containing Dimesitylboron Groups as PeT-Based Fluorescent Probes for Fluoride. *J. Phys. Chem. C* **2011**, *115*, 19947–19954.
- (54) Yin, Z.; Tam, A. Y.; Wong, K. M.; Tao, C. H.; Li, B.; Poon, C. T.; Wu, L.; Yam, V. W. Functionalized BODIPY with various sensory units—a versatile colorimetric and luminescent probe for pH and ions. *Dalton Trans.* **2012**, *41*, 11340–50.
- (55) P, P. C. S.; Priyanka, R. N.; Thilagar, P. Triarylborane-dipyromethane conjugates bearing dual receptor sites: the synthesis and evaluation of the anion binding site preference. *Dalton Trans.* **2014**, *43*, 4067–4075.
- (56) Swamy P, C. A.; Priyanka, R. N.; Mukherjee, S.; Thilagar, P. Panchromatic Borane-aza-BODIPY Conjugate: Synthesis, Intriguing Optical Properties, and Selective Fluorescent Sensing of Fluoride Anions. *Eur. J. Inorg. Chem.* **2015**, *2015*, 2338–2344.
- (57) Misra, R.; Jadhav, T.; Dhokale, B.; Mobin, S. M. Colorimetric and fluorimetric detection of fluoride and cyanide ions using tri and tetra coordinated boron containing chromophores. *Dalton Trans.* **2015**, *44*, 16052–16060.
- (58) Sarkar, S. K.; Kumar, G. R.; Thilagar, P. White light emissive molecular siblings. *Chem. Commun.* **2016**, *52*, 4175–8.
- (59) Swamy, C. A.; Mukherjee, S.; Thilagar, P. Dual emissive borane-BODIPY dyads: Molecular conformation control over electronic properties and fluorescence response towards fluoride ions. *Chem. Commun.* **2013**, *49*, 993–995.
- (60) Swamy, C. A. P. *Design and Syntheses of Triarylborane Decorated Luminescent Dyes: Intriguing Optical Properties and Anion Sensing Applications*. PhD Thesis, Indian Institute of Science, Bangalore, India, 2014.
- (61) Kumar, G. R.; Thilagar, P. Triarylborane conjugated acacH ligands and their BF₂ complexes: facile synthesis and intriguing optical properties. *Dalton Trans.* **2014**, *43*, 3871–3879.
- (62) Frisch, M. J.; Trucks, G. W.; Schlegel, H. B.; Scuseria, G. E.; Robb, M. A.; Cheeseman, J. R.; Scalmani, G.; Barone, V.; Petersson, G. A.; Nakatsuji, H.; Li, X.; Caricato, M.; Marenich, A. V.; Bloino, J.; Janesko, B. G.; Gomperts, R.; Mennucci, B.; Hratchian, H. P.; Ortiz, J. V.; Izmaylov, A. F.; Sonnenberg, J. L.; Williams-Young, D.; Ding, F.; Lipparini, F.; Egidi, F.; Goings, J.; Peng, B.; Petrone, A.; Henderson, T.; Ranasinghe, D.; Zakrzewski, V. G.; Gao, J.; Rega, N.; Zheng, G.; Liang, W.; Hada, M.; Ehara, M.; Toyota, K.; Fukuda, R.; Hasegawa, J.; Ishida, M.; Nakajima, T.; Honda, Y.; Kitao, O.; Nakai, H.; Vreven, T.; Throssell, K.; Montgomery, Jr., J. A.; Peralta, J. E.; Ogliaro, F.; Bearpark, M. J.; Heyd, J. J.; Brothers, E. N.; Kudin, K. N.; Staroverov, V. N.; Keith, T. A.; Kobayashi, R.; Normand, J.; Raghavachari, K.; Rendell, A. P.; Burant, J. C.; Iyengar, S. S.; Tomasi, J.; Cossi, M.; Millam, J. M.; Klene, M.; Adamo, C.; Cammi, R.; Ochterski, J. W.; Martin, R. L.; Morokuma, K.; Farkas, O.; Foresman, J. B.; Fox, D. J. *Gaussian 09*; Gaussian, Inc.: Wallingford, CT, 2009.
- (63) Sakamoto, K.; Takashima, Y.; Hamada, N.; Ichida, H.; Yamaguchi, H.; Yamamoto, H.; Harada, A. Selective photoinduced energy transfer from a thiophene rotaxane to acceptor. *Org. Lett.* **2011**, *13*, 672–5.
- (64) Atilgan, S.; Ozdemir, T.; Akkaya, E. U. Selective Hg(II) sensing with improved Stokes shift by coupling the internal charge transfer process to excitation energy transfer. *Org. Lett.* **2010**, *12*, 4792–5.
- (65) Liu, J. Y.; Yeung, H. S.; Xu, W.; Li, X.; Ng, D. K. Highly efficient energy transfer in subphthalocyanine-BODIPY conjugates. *Org. Lett.* **2008**, *10*, 5421–4.
- (66) Hildebrandt, N., How to Apply FRET: From Experimental Design to Data Analysis. In *FRET - Förster Resonance Energy Transfer*; Medintz, I., Hildebrandt, N., Eds.; Wiley-VCH Verlag GmbH & Co. KGaA: Weinheim, Germany, 2013; pp 105–163.
- (67) Richards, V. J.; Gower, A. L.; Smith, J. E.; Davies, E. S.; Lahaye, D.; Slater, A. G.; Lewis, W.; Blake, A. J.; Champness, N. R.; Kays, D. L. Synthesis and characterisation of BODIPY radical anions. *Chem. Commun.* **2012**, *48*, 1751.
- (68) Cummings, S. A.; Iimura, M.; Harlan, C. J.; Kwaan, R. J.; Trieu, I. V.; Norton, J. R.; Bridgewater, B. M.; Jäkle, F.; Sundararaman, A.; Tilsted, M. An Estimate of the Reduction Potential of B(C₆F₅)₃ from Electrochemical Measurements on Related Mesityl Boranes. *Organometallics* **2006**, *25*, 1565–1568.